NIH Public Access
Author Manuscript
Biochemistry. Author manuscript; available in PMC 2008 October 16.

Published in final edited form as:
Biochemistry. 2007 October 16; 46(41): 11559–11567. doi:10.1021/bi7011614.

Structural and Thermodynamic Consequences of 1-(4-Chlorophenyl)imidazole Binding to Cytochrome P450 2B4[†,‡]

Yonghong Zhao[§,‖], **Ling Sun**[§], **B. K. Muralidhara**[§,¶], **Santosh Kumar**[§], **Mark A. White**[⊥], **C. David Stout**[#], and **James R. Halpert**[*,§]

§*Department of Pharmacology and Toxicology, University of Texas Medical Branch, 301 University Boulevard, Galveston, Texas 77555-1031*

⊥*Sealy Center for Structural Biology and Molecular Biophysics, University of Texas Medical Branch, 301 University Boulevard, Galveston, Texas 77555*

#*Department of Molecular Biology, The Scripps Research Institute, La Jolla, CA 92037*

Abstract

The crystal structure of P450 2B4 bound with 1-(4-chlorophenyl)imidazole (1-CPI) has been determined to delineate the structural basis for the observed differences in binding affinity and thermodynamics relative to 4-(4-chlorophenyl)imidazole (4-CPI). Compared with the previously reported 4-CPI complex, there is a shift in the 1-CPI complex of the protein backbone in helices F and I, repositioning the side chains of Phe-206, Phe-297, and Glu-301, and leading to significant reshaping of the active site. Phe-206 and Phe-297 exchange positions, with Phe-206 becoming a ligand-contact residue, while Glu-301, rather than hydrogen bonding to the ligand, flips away from the active site and interacts with His-172. As a result the active site volume expands from 200 $Å^3$ in the 4-CPI complex to 280 $Å^3$ in the 1-CPI complex. Based on the two structures, it was predicted that a Phe-206->Ala substitution would alter 1-CPI but not 4-CPI binding. Isothermal titration calorimetry experiments indicated that this substitution had no effect on the thermodynamic signature of 4-CPI binding to 2B4. In contrast, relative to wild-type 1-CPI binding to F206A showed significantly less favorable entropy but more favorable enthalpy. This result is consistent with loss of the aromatic side chain and possible ordering of water molecules, now able to interact with Glu-301 and exposed residues in the I-helix. Hence, thermodynamic measurements support the active site rearrangement observed in the crystal structure of the 1-CPI complex and illustrate the malleability of the active site with the fine tuning of residue orientations and thermodynamic signatures.

Cytochromes P450 of the 1, 2, and 3 families play a central role in drug metabolism and detoxification (1). Many P450s display broad and overlapping substrate specificities, yet an individual P450 often oxidizes a particular substrate with striking regio- and/or stereo-selectivity. The importance of P450s in healthcare has led to an intense interest in developing

[†]This work was supported by NIH Grants ES03619 (to J. R. H.), GM61545 (to C. D. S.), and Center Grant ES06676 (to J. R. H.). Yonghong Zhao was supported by NIEHS Training Grant T32 ES07254. The Stanford Synchrotron Radiation Laboratory is operated by Stanford University on behalf of the United States Department of Energy, Office of Basic Energy Sciences. The Stanford Synchrotron Radiation Laboratory Structural Molecular Biology Program is supported by the Department of Energy, Office of Biological and Environmental Research, and by the National Center for Research Resources, Biomedical Technology Program, and the National Institute of General Medical Sciences, National Institutes of Health. The Sealy Center for Structural Biology and Molecular Biophysics is supported by the Sealy and Smith Foundation for Medical Research.

[‡]Atomic coordinates have been deposited in the Protein Data Bank as entry 2Q6N.

*Corresponding author. Tel. (409) 772-9678. Fax (409) 772-5732. jhalpert@utmb.edu.
[‖]Present address: Centocor Inc., 145 King of Prussia Road, Radnor, PA 19087
[¶]Present address: Pfizer Inc., PhRD-Global Biologics, 700 Chesterfield Parkway West, Chesterfield, MO 63017

NIH-PA Author Manuscript
NIH-PA Author Manuscript
NIH-PA Author Manuscript

NIH-PA Author Manuscript

NIH-PA Author Manuscript

NIH-PA Author Manuscript

strategies to predict the metabolic fate of pharmaceuticals and environmental pollutants, which requires a detailed knowledge of P450 structure-function relationships. Compared with several other P450 subfamilies, P450 2B enzymes exhibit a relatively low degree of catalytic preservation across mammalian species, making these enzymes an outstanding model system for investigating structure-function relationships (2).

Recent results demonstrate that microsomal P450s exhibit remarkable conformational diversity and plasticity (3,4), including significant differences both in the length of helices and in their positions. Such differences exist even among P450s such as 2C5, 2C8, and 2C9 from the same subfamily. The most striking example of conformational plasticity of a single P450 is represented by the structures of 2B4[1] solved in three different states by our laboratory (5–7). The N-terminal truncated and modified 2B4 was crystallized in the ligand-free, 4-(4-chlorophenyl)imidazole (4-CPI)-bound, and bifonazole-bound forms, which exhibit dramatically different conformations. Conformational plasticity of microsomal P450 suggests an “induced fit” mechanism for ligand binding. In P450 2B4, plastic regions of the enzyme include the N-terminal half of helix A, helix B’ through helix C, the C-terminal half of helix E, the C-terminal half of helix F though the N-terminal half of helix I, and the β4 hairpin (7). These structural elements either directly make contact with the ligand or form new intramolecular contacts that stabilize the conformation of enzyme bound with the ligand. By adapting to different conformations, the enzyme is able to reshape its active site to accommodate the bound ligand without perturbing the overall P450 fold. Recent structures of P450 3A4 complexed with ketoconazole or erythromycin (8) provide further evidence in support of this concept.

While a crystal structure gives a snapshot of the protein, biophysical approaches can provide fruitful information on protein conformation in solution. With the availability of multiple mammalian P450 structures there has been a recent surge in the use of computer modeling and molecular simulations to predict quantitative structure-activity relationships (QSAR) of P450-ligand interactions (9). Such information can be used for optimization of the design of new drug molecules with desirable metabolic properties. However, the validity of molecular models based on static crystal structures is limited by the lack of corroborative solution thermodynamic data. Recently, conformations of P450 2B4 in binding imidazole inhibitors of different size and side chain chemistry were studied in solution using isothermal titration calorimetry (ITC) and fluorescence spectroscopy (10). The results show that P450 2B4 exhibits a large degree of conformational flexibility depending on the bound ligand. In addition, ITC studies reveal that thermodynamic parameters of binding can be distinctly different for structurally similar compounds such as 4-CPI and 1-(4-chlorophenyl)imidazole (1-CPI) (Figure 1), suggesting that they induce different active site conformations. In order to probe the structural basis and the interplay of active site residues responsible for the less favorable entropy of 1-CPI vs. 4-CPI binding, the crystal structure of the 1-CPI complex was determined.

Although the overall protein fold is highly similar to that of the 4-CPI complex, there is a significant rearrangement of the active site, demonstrating how the enzyme accommodates structurally similar ligands with different chemical features. ITC studies of the F206A mutant validated the role of this residue in 1-CPI but not 4-CPI binding, as indicated by the crystal structures. The combination of x-ray crystallography and ITC should be especially powerful for elucidating the details of substrate binding by the conformationally diverse microsomal P450 enzymes.

[1]Abbreviations: P450 2B4, Cytochrome P450 2B4; 2B4dH(H226Y), an N-terminal truncated and modified and C-terminal His-tagged form of P450 2B4 engineered for enhanced solubility and containing a His-226 -> Tyr substitution to prevent dimerization; 7-EFC, 7-Ethoxy-4-(trifluoromethyl)coumarin; 1-CPI, 1-(4-Chlorophenyl)imidazole; 4CPI, 4-(4-Chlorophenyl)imidazole; LLG, Log Likelihood Gain; NCS, non-crystallographic symmetry; 1-PI, 1-Phenylimidazole; 4-PI, 4-Phenylimidazole; ITC, Isothermal titration calorimetry; SASA, solvent accessible surface area.

NIH-PA Author Manuscript

NIH-PA Author Manuscript

NIH-PA Author Manuscript

Materials and Methods

Mutagenesis

F206A was created using 2B4dH(H226Y) as a template, and 5'- TTG TTC TTC CAG TCC **GCC** TCC CTC ATC AGC TCC-3' and 5'- GGA GCT GAT GAG GGA **GGC** GGA CTG GAA GAA CAA -3' as forward and reverse primers, respectively, using the QuikChange XL site-directed mutagenesis kit (Stratagene, La Jolla, CA). Nucleotides in bold indicate the site of mutation. The mutation and lack of extraneous mutations were confirmed by DNA sequence determination at the Protein Chemistry Laboratory Core, UTMB.

Protein expression and purification

Cytochrome P450 2B4dH(H226Y) and F206A were expressed and purified as described previously (5–7). Briefly, *Escherichia* coli transformed with the vector pKK2B4dH(H226Y) or F206A was grown at 37 °C with shaking until the A_{600} reached 1.0. Protein expression was induced by the addition of isopropyl-1-thio-b-D-galactopyranoside to δ-aminolevulinic acid-supplemented Terrific broth. After an induction period of 48–72 hours, the cells were harvested and lysed. P450 2B4dH(H226Y) and F206A were extracted from membranes by adding the detergent Cymal-5 (Anatrace, Maumee, OH) in high salt buffer. After ultracentrifugation, the supernatant was purified using metal-affinity chromatography first. The fractions containing P450 were pooled together and then further purified by ion-exchange chromatography. The final buffer contained 500 mM NaCl, 8% glycerol, 1 mM EDTA, 1 mM dithiothreitol, and 10 mM potassium phosphate, pH 7.4. For crystallization, 1-CPI (Sigma) was added to the purified P450 2B4dH(H226Y) in 10-fold excess, and the complex was concentrated using an Ultra-15 centrifugal device (Millipore, Billerica, MA).

Ligand binding by difference spectral titration

Difference spectra were recorded using 1 μM protein on a Shimadzu-2600 spectrophotometer at 25 °C as described (10). Briefly, protein sample (3 mL) was divided into two matched quartz cuvettes and the difference spectra were recorded between 350–500 nm following the addition to the sample cuvette of a series of 2 μL aliquots of ligand, which was freshly prepared as a 200 μM stock in ethanol. The same volume of ethanol was added to the reference cuvette. Differential absorbance maxima for inhibitors [ΔA_{max} of (431 nm − 400 nm)] binding were fit to the tight-binding equation to derive K_S values (KaleidaGraph, Synergy Software).

Isothermal titration calorimetric (ITC) experiments and data analysis

ITC experiments with inhibitors were performed on a VP-ITC calorimeter interfaced with a computer for data acquisition and analysis using Origin 7 software (Microcal Inc., Northampton, MA) as described previously using 60 μM protein in the cell and 2 mM inhibitor in the syringe (10). Protein and ligand samples were pre-incubated to the required temperature using a ThermoVac (Microcal Inc.) and loaded into the calorimeter. A typical titration schedule included addition of 4 μL per injection of ligand with 12–15 injections spaced at 5-minute intervals. The titration cell was continuously stirred at 300 rpm. There is a time lag of about 5–20 min to reach the steady baseline enthalpy after the stirring has been initiated and the beginning of injections. During this time lag the ligand (2 mM) at the tip of the syringe gets diluted by diffusion, and the initial 1–2 μL volume does not represent an exact concentration of ligand in the syringe. To minimize this error, for the first injection only, 2 μL of ligand was added and the corresponding data point was deleted from the analysis. The interested reader is referred to the VP-ITC section at www.microcalorimetry.com for experimental set up and data analysis. Reference titrations were carried out by injecting each ligand into buffer alone in the calorimetric cell, and heat of dilution was subtracted from the ligand-protein titration data. The binding isotherms were best-fit to a one-set binding-site model by Marquardt non-

NIH-PA Author Manuscript

NIH-PA Author Manuscript

NIH-PA Author Manuscript

linear least-square analysis to obtain binding stoichiometry (N), association constant (K_a) and thermodynamic parameters of interaction using Origin 7.0 software (Microcal Inc.) (11). The dissociation constant (K_D) was derived from K_a as $K_D = 1/K_a$.

Structure Determination and Analysis

The protein sample was prepared as a 33 mg/mL stock in buffer containing 500 mM NaCl, 8% glycerol, 1 mM EDTA, 1 mM dithiothreitol, 1 mM 1-CPI, 4.8 mM Cymal-5, and 10 mM potassium phosphate, pH 7.4. The 2B4/1-CPI complex was crystallized from vapor diffusion hanging drops in which 2 μL of protein sample was mixed with 0.5 μL 1 M guanidine hydrochloride (GuHCl) and 2 μL of reservoir buffer containing 5% MPD, 10–12% PEG 6000, and 0.1 M HEPES, pH 7.0. The drops were equilibrated against 500 μL of the reservoir under 300 μL mineral oil at 18 °C, and crystals grew to a size of about 0.25 × 0.2 × 0.1 mm in 3–5 days. For data collection, crystals were briefly soaked in the mother liquor supplemented with 15% glycerol and 15% ethylene glycol, followed by flash freezing in liquid N_2.

Two data sets were collected, each from a single crystal, respectively. For each data set, four hundred frames (0.25°/frame) were collected on a single crystal held at 100 K to a resolution of 3.2 Å at beam line 11-1 of the Stanford Synchrotron Radiation Laboratory using a Quantum-315 CCD detector (Area Detector Systems Corp.). MOSFLM (11) and SCALA (12) were used to process the frames, and data collection and processing statistics of two dataset are shown in Table 1.

Preliminary crystallographic analysis indicated that 2B4/1-CPI crystals belong to space group $P2_12_12_1$. The Mathews coefficient suggested that there were probably 6–11 molecules in an asymmetric unit. A molecular replacement search model was constructed by making an ensemble from the ligand-free 2B4 structure (5), the 2B4/4-CPI structure (6), and the 2B4-bifonazole structure (7) using the PHASER program (13). Initially, a molecular solution with 6 molecules in an asymmetric unit was identified with a Log Likelihood Gain (LLG) of 4786. The six molecules form a hexamer that has 32-point group symmetry, which was consistent with the self-rotation function. The hexamer was subjected to rigid body refinement using the CNS program (14), and the resulting R-factor was 36.8%. Visual inspection of the model indicated that there were large gaps between hexamers in the unit cell. When an electron density map was calculated using the hexamer after rigid-body refinement, the map indicated that there were protein-like densities present in the gaps. Subsequently, the PHASER program was used to search for additional molecules in the asymmetric unit. A seventh molecule was identified, and the LLG was 6378. The seventh molecule bridged the hexamer in the unit cell and fit the densities in the map calculated from the hexamer.

The molecular replacement solution from PHASER was used for rigid body refinement in CNS (14), which resulted an R-factor of 33.8% and R-free of 35.0%. An electron density map was calculated using the phasing information from the initial protein model. Most of the protein backbone could be traced, and the electron density of the inhibitor in the active site was visible. However, multiple regions including the C/D loop, helix F, and the middle of helix I did not fit the density. These were rebuilt manually into the map using the COOT program (15). Cycles of model building and minimization in CNS were performed to refine the coordinates. Seven-fold noncrystallographic symmetry (NCS) restraints were used in initial rounds of refinement but were gradually released as the model improved. The final model was refined without NCS restraints. The structural topology and parameters of 1-CPI were generated using the PRODRG web server (16). 1-CPI molecules were fit into unbiased |Fo|-|Fc| maps, and added into the model after most of the protein residues were well defined. The refinement was repeated with another dataset collected from a different crystal, which is in the same space group (Table 1). It yielded a very similar structure with the RMSD's between corresponding chains less than 0.6 Å for all Ca atoms (crystal 1:chain A – crystal 2:chain A 0.36 Å, 1B – 2B 0.39 Å, 1C – 2C

NIH-PA Author Manuscript

NIH-PA Author Manuscript

NIH-PA Author Manuscript

0.43 Å, 1D – 2D 0.38 Å, 1E – 2E 0.44 Å, 1F – 2F 0.48 Å, 1G – 2G 0.54 Å). The electron density for the active site residues and the 1-CPI ligands in all seven molecules in the asymmetric unit was very similar to that in maps calculated using the first data set (data not shown). Refinement and model statistics for both structures are shown in Table 1. The atomic coordinates refined with dataset collected from crystal 1 have been deposited in the Protein Data Bank (accession code 2Q6N). The active site volume of P450s was calculated using the program VOIDOO (17).

Results

The seven molecules (Figure 2A) in the asymmetric unit form a hexamer (molecules A to F, Figure 2B) with molecule G bridging hexamers in the unit cell. The hexamer has 32-point group symmetry and consists of two trimers composed of molecules A–C and D–F, respectively. Approximately 2100 $Å^2$ of solvent accessible surface area (SASA) is buried upon formation of each trimer, and dimerization of two trimers further buries ~2300 $Å^2$ of SASA (18). Molecule G associates with the hexamer through molecule C, burying ~560 $Å^2$ of SASA. At the center of each trimer, hydrophobic residues F212, V216, F220, F223, L224, F227, and P228 in the F/G region of each molecule make contact with symmetry-related residues of adjacent molecules (Figure 2C). Three molecules in a trimer are oriented with their N-termini pointing in the same direction, while their C-termini are buried upon dimerization of two trimers (Figure 2B). Crystallization of the 1-CPI complex with seven molecules in the asymmetric unit could arise from co-crystallization of roughly equal concentrations of hexamers and monomers. For example in the case of rat 2B1dH, a 50/50 mixture of hexamers and monomers exists in 0.1% cholate, 100% hexamers in the absence of detergent, and 100% monomers in 0.25% cholate (19). The quaternary structure observed for the 2B4/1-CPI complex is in accord with negative stain electron microscopy studies of this P450, which also shows a hexameric assembly with 32-point group symmetry (20).

The seven molecules in the asymmetric unit exhibit a similar conformation, and there is no significant difference among the 7 chains (main chain RMSD 0.7 Å or less). Overall, the structure of 2B4 complexed with 1-CPI shows the characteristic P450 fold (Figure 3). The lengths and orientations of the individual secondary structural elements are very similar to these seen in the 2B4/4-CPI complex.

Iterative rounds of modeling building and refinement with and without NCS restraints resulted in clean electron density maps, which defined the orientation of 1-CPI and side chains of ligand-contacting residues (Figure 4A and Figure 4B). In the hexamer, electron densities of 1-CPI in molecules B, C, D, E, and F are similar to those of 1-CPI in molecule A (Figure 4A), while the electron density of 1-CPI in molecule G (Figure 4B) is relatively weak. The ligand is oriented in the active site with an imidazole nitrogen coordinated to the heme iron (Figure 4C). The long axis of 1-CPI is at an angle of ~70° to the plane of the heme, leaning toward helix B'. 1-CPI is constrained on all sides by 12 residues (I101, V104, I114, F115, F206, I209, F297, A298, T302, I363, V367, V477), which all have hydrophobic side chains except Thr-302 (Figure 4C). Immediately above the plane of the heme, the imidazole ring of 1-CPI is surrounded by the side chains of Ile-114, Ala-298, Thr-302, and Ile-363. Above the imidazole ring, the phenyl ring interacts with the side chains of residues Ile-101, Phe-115, Phe-206, Phe-297, Val-367, and Val-477. On the top, Val-104 and Ile-209 form the ceiling of the active site. Refinement of the model against an independent data set (Table 1) yielded a very similar structure, confirming the conformation of 1-CPI and ligand-contacting residues.

Although the overall tertiary structure of 2B4/1-CPI complex is very similar to that of the 4-CPI complex, there are significant rearrangements of structural elements that form the active site (Figure 5A). In the 2B4/4-CPI structure, the side chain of Glu-301 is oriented toward the

NIH-PA Author Manuscript

NIH-PA Author Manuscript

NIH-PA Author Manuscript

ligand and forms a hydrogen bond with the free nitrogen of the imidazole. In the 2B4/1-CPI structure, the side chain of Glu-301 is oriented away from 1-CPI, and the new conformation of Glu-301 is stabilized by its interaction with the side chain of His-172. A similar conformation of Glu-301 and His-172 is seen in the 2B4/bifonazole structure (7). These structures suggest that Glu-301 plays an important role in changing the polarity of the 2B4 active site near the heme iron. In addition, the side chain of Phe-206 is oriented toward 1-CPI, making aromatic interactions with 1-CPI and Phe-297. Conformational changes of the side chains of Phe-206, Phe-297, and Glu-301 are accompanied by a shift of the protein backbone in the central part of helix I and helix F (Figure 5A). Compared with the 2B4/4-CPI structure, the structural changes described above are consistently observed in all 7 protein molecules in the asymmetric unit (Figure 5B). On the other side of the active site, opposite to helix I, there is almost no structural rearrangement of residues I101, V104, I114, and F115 (Figure 5A), nor of residues I363 and V367. The heme-coordinating residues also remain unchanged (Figure 5C).

To further study the role of Phe-206 in ligand binding, the mutant F206A was constructed using 2B4dH(H226Y) as the template. The expression level of F206A was similar to that of the template, allowing purification of the protein for biochemical and biophysical studies. F206A has significantly lower activity than 2B4dH(H226Y) toward 7-EFC (data not shown), and therefore, the kinetic parameters (k_{cat} and K_m) could not be determined. In addition, 2B4dH (H226Y) or F206A did not show a detectible spectral change (type I), which precluded determination of substrate binding affinity using a spectral titration method. The low activity of F206A with 7-EFC is reminiscent of the low activity of the F206L mutant in the related enzyme P450 2B1 with a similar compound 7-ethoxycoumarin (21). The effect of the Phe-206->Ala substitution on 4-CPI and 1-CPI binding was investigated in spectral titration and ITC experiments (Figure 6A and Figure 6B). The K_S value for 4-CPI binding to F206A was the same as for the template (10), whereas the K_S for 1-CPI binding to the F206A was ~30% higher than to 2B4dH(H226Y) (Table 2). The thermodynamic signatures of 4-CPI binding to 2B4dH (H226Y) and F206A are very similar (Figure 6C), exhibiting both favorable enthalpy and entropy terms and 1:1 binding stoichiometry. In contrast, the thermodynamic signatures of 1-CPI binding to 2B4dH(H226Y) and F206A are strikingly different (Figure 6C). Entropically, 1-CPI binding to F206A is much more unfavorable by 3.2 kcal/mol than binding to 2B4dH (H226Y) ($-T\Delta S$ = 3.3 kcal/mol vs. 0.1 kcal/mol).

Discussion

One of the most important and obvious differences between the two chlorophenylimidazoles is that once bound to the enzyme, the 4-isomer has one free nitrogen atom, while the 1-isomer has none. This difference affects the binding to P450s significantly. For comparison, the dissociation constants of 1- and 4-phenylimidazole with P450cam are very different, 0.1 μM for 1-phenylimidazole (1-PI) and 40 μM for 4-phenylimidazole (4-PI) (22). Poulos and Howard have solved the crystal structures of P450cam with 1- and 4-phenylimidazole and provided an explanation for the selectivity (22). The free N3 of 4-phenylimidazole does not form a hydrogen bond with the enzyme and remains essentially “unsolvated”. Thus, transfer of the 4-phenylimidazole from solution to the active site of P450cam is thermodynamically less favorable than the corresponding transfer of 1-phenylimidazole, which has no free unliganded nitrogen atom.

Interestingly, the binding of 1- and 4-(4-chlorophenyl)imidazole (or 1- and 4-phenylimidazole) to P450 2B4 represents a completely different situation. The 4-isomers (K_S of 0.043 μM for 4-CPI and 0.132 μM for 4-PI) bind to 2B4dH(H226Y) with higher affinity than their corresponding 1-isomers (K_S of 0.125 μM for 1-CPI and 0.486 μM for 1-PI) (10). The 2B4/4-CPI and 2B4/1-CPI structures provide an explanation for the difference and demonstrate the remarkable malleability of a mammalian microsomal P450 to accommodate diverse ligands

NIH-PA Author Manuscript

NIH-PA Author Manuscript

NIH-PA Author Manuscript

with subtle rearrangements of the active site. In the active site of the 2B4/1-CPI structure the ligand is packed by 12 residues, which all have hydrophobic side chains except Thr-302. The favorable interactions between 1-CPI and 2B4 contribute to the high affinity, which is the same as that of 1-PI binding to P450cam. For the bacterial P450cam, the structures of 1-PI and 4-PI complexes are almost identical. As a result, 4-PI binding to P450cam is penalized for burial of its free N-H in the hydrophobic active site, resulting in a lower affinity (K_D = 40 μM).

In contrast, the crystal structures of 2B4 show that this mammalian enzyme is more versatile with a plastic active site. When 4-CPI binds to 2B4, the side chain of Glu-301 swings in and forms a hydrogen bond with the ligand. In this case, the free N-H of 4-CPI is not detrimental to complex formation. Indeed, a network of 8 hydrogen bonds is formed (Figure 6D) among 4-CPI, two waters (HOH-1107 and HOH-1147 in PDB entry 1SUO), and 5 amino acid residues (Glu-301, Thr-302, Thr-305, Leu-362, and Asn-479), which probably contributes to the high affinity. It is not possible to form this H-bond network in the 2B4/1-CPI complex because 1-CPI has no free nitrogen atom for hydrogen bonding, and the new position of Phe-206 displaces two water molecules. In addition to Glu-301, the side chains of Phe-206 and Phe-297 are oriented differently in the two chlorophenylimidazole complexes, which is accompanied by protein backbone shift in the middle of helices F and I. The overall result is a more compact active site (volume 200 $Å^3$) where 4-CPI is strictly constrained by active site residues on all sides vs. 280 $Å^3$ in the 2B4/1-CPI structure.

Recently advances in protein preparation and experimental techniques allowed measurements of thermodynamic of P450-ligand interactions using ITC (10). Since ITC can dissect free energy of binding (ΔG) into enthalpy (ΔH) and entropy terms ($-T\Delta S$), it has revealed the thermodynamic difference of P450 2B4 in binding imidazole inhibitors with different ring chemistry and side chains (10). Both 4-CPI and 1-CPI bind to the enzyme with a favorable enthalpy term, −6.48 kcal/mol and −8.15 kcal/mol, respectively. The enhanced enthalpy for 1-CPI vs. 4-CPI binding is consistent with the Glu-301 – His-172 interaction, which has more ionic character than hydrogen bonds to 4-CPI or Thr-302. However, it should be noted that due to the associated shift of the F- and I-helices, many other residues, including Phe-206 and Phe-297, also experience new environments in the 1-CPI complex.

However, 4-CPI binding to 2B4dH(H226Y) was shown to be entropically favorable ($-T\Delta S$ = −1.75 kcal/mol), while 1-CPI binding to the enzyme is less favorable and has a very small entropy ($-T\Delta S$ = 0.1 kcal/mol). Thermodynamically, the hydrophobic effect is entropically favorable, due to desolvation, while loss of conformational freedom (both the ligand and the protein) is entropically unfavorable in protein-ligand interactions. The tight packing of 4-CPI within the active site (200 $Å^3$) favors desolvation of the ligand and displacement of H_2O from the heme, outweighing the loss of conformational freedom upon binding. The result is a net entropic contribution ($-T\Delta S$ = −1.75 kcal/mol) to free energy of 4-CPI binding. In contrast, when 1-CPI binds to 2B4, the volume occupied remains larger (280 $Å^3$) and less net desolvation occurs, resulting in an entropy term close to zero.

Among the active site residues, Phe-206 exhibits the most dramatic conformational change between the 2B4/1-CPI and 4-CPI structures (Figure 5A). Substituting Ala for Phe-206 does not affect the affinity of 4-CPI binding in spectral titration (K_S) or ITC (ΔG) experiments, nor does it alter the thermodynamic signatures, consistent with the buried position of Phe-206. The mutation also has minimal impact on the ΔG of 1-CPI binding; however, this arises from significantly altered enthalpic and entropic contributions (Figure 6C). A similar value for ΔG is consistent with our earlier studies; i.e. most single amino acid substitutions do not significantly alter the overall binding affinity of P450 2B4 with imidazole inhibitors due to the strong interaction between the imidazole nitrogen and the heme iron, which dominates the binding (23). Nevertheless, ITC experiments revealed significant differences in 1-CPI binding

NIH-PA Author Manuscript

NIH-PA Author Manuscript

NIH-PA Author Manuscript

to the F206A mutant compared with the template: the enthalpic term becomes much more negative ($\Delta H = -10.9$ kcal/mol) while the entropic term becomes much more positive ($-T\Delta S = 3.3$ kcal/mole). The enthalpic change can be explained by possible binding of H_2O molecules in the active site in place of the missing Phe-206 side chain, where the H_2O could form hydrogen bonds with the new position of Glu-301, exposed residues in helix I (Thr-302, Thr-305), and the main chain carbonyl of Leu-362 and Asn-479. Two such H_2O molecules that are involved in forming the network of 8 hydrogen bonds (Figure 6D) are observed in the 2B4/4-CPI structure where they are not occluded by the positions of Phe-206 or Phe-297 (6). Even though the substitution of Ala for Phe-206, which is likely to loosen the packing interaction of active site residues around the phenyl ring of 1-CPI, increases the degrees of freedom for the protein-ligand complex, the ordering of H_2O molecules from the solvent apparently outweighs this effect, resulting in a significant overall loss of entropy.

In conclusion, we have determined the crystal structure of P450 2B4 bound with 1-CPI Compared with the 2B4/4-CPI structure, there are several key rearrangements within the active site, which complement the subtle but distinct chemical difference of the ligand. The thermodynamic signatures of 4-CPI and 1-CPI binding to 2B4 obtained previously can be interpreted based on the observed structural rearrangement, delineating the structural origin of differential thermodynamics. In a synergistic approach, we went back from the crystal structures to solution thermodynamics with the studies on the F206A mutant. ITC experiments on the F206A mutant further support a structure in which loss of a single hydrogen bond from Glu-301 to the ligand results in reorientation of Glu-301 away from the active site with concomitant exchange in the position of Phe-206, and repacking of Phe-297, leading to an expanded active site.

REFERENCES

1. Rendic S. Summary of information on human CYP enzymes: Human P450 metabolism data. Drug Metabolism Reviews 2002;34:83–448. [PubMed: 11996015]
2. Zhao Y, Halpert JR. Structure-function analysis of cytochromes P450 2B. Biochim. Biophys. Acta 2007;1770:402–412. [PubMed: 16935426]
3. Johnson EF, Stout CD. Structural diversity of human xenobiotic-metabolizing cytochrome P450 monooxygenases. Biochem. Biophys. Res. Commun 2005;338:331–336. [PubMed: 16157296]
4. Poulos TL. Structural and functional diversity in heme monooxygenases. Drug Metab. Dispos 2005;33:10–18. [PubMed: 15475411]
5. Scott EE, He YA, Wester MR, White MA, Chin CC, Halpert JR, Johnson EF, Stout CD. An open conformation of mammalian cytochrome P4502B4 at 1.6-angstrom resolution. Proc. Natl. Acad. Sci. U. S. A 2003;100:13196–13201. [PubMed: 14563924]
6. Scott EE, White MA, He YA, Johnson EF, Stout CD, Halpert JR. Structure of mammalian cytochrome P4502B4 complexed with 4-(4- chlorophenyl) imidazole at 1.9-angstrom resolution - Insight into the range of P450 conformations and the coordination of redox partner binding. J. Biol. Chem 2004;279:27294–27301. [PubMed: 15100217]
7. Zhao Y, White MA, Muralidhara BK, Sun L, Halpert JR, Stout CD. Structure of microsomal cytochrome P450 2B4 complexed with the antifungal drug bifonazole insight into P450 conformational plasticity and membrane interaction. J. Biol. Chem 2006;281:5973–5981. [PubMed: 16373351]
8. Ekroos M, Sjogren T. Structural basis for ligand promiscuity in cytochrome P450 3A4. Proc. Natl. Acad. Sci. U. S. A 2006;103:13682–13687. [PubMed: 16954191]
9. Norinder U. In silico modelling of ADMET - A minireview of work from 2000 to 2004. SAR and QSAR in Environmental Research 2005;16:1–11. [PubMed: 15844440]
10. Muralidhara BK, Negi S, Chin CC, Braun W, Halpert JR. Conformational flexibility of mammalian cytochrome P450 2B4 in binding imidazole inhibitors with different ring chemistry and side chains. Solution thermodynamics and molecular modeling. J. Biol. Chem 2006;281:8051–8061. [PubMed: 16439365]

NIH-PA Author Manuscript

NIH-PA Author Manuscript

NIH-PA Author Manuscript

11. Leslie AGW. Integration of macromolecular diffraction data. Acta Crystallogr. D Biol. Crystallogr 1999;55:1696–1702. [PubMed: 10531519]
12. Bailey S. The Ccp4 Suite - Programs for Protein Crystallography. Acta Crystallogr. D Biol. Crystallogr 1994;50:760–763. [PubMed: 15299374]
13. McCoy AJ, Grosse-Kunstleve RW, Storoni LC, Read RJ. Likelihood-enhanced fast translation functions. Acta Crystallogr. D Biol. Crystallogr 2005;61:458–464. [PubMed: 15805601]
14. Brunger AT, Adams PD, Clore GM, DeLano WL, Gros P, Grosse-Kunstleve RW, Jiang JS, Kuszewski J, Nilges M, Pannu NS, Read RJ, Rice LM, Simonson T, Warren GL. Crystallography & NMR system: A new software suite for macromolecular structure determination. Acta Crystallogr. D Biol. Crystallogr 1998;54:905–921. [PubMed: 9757107]
15. Emsley P, Cowtan K. Coot: model-building tools for molecular graphics. Acta Crystallogr. D Biol. Crystallogr 2004;60:2126–2132. [PubMed: 15572765]
16. Schuttelkopf AW, van Aalten DMF. PRODRG: a tool for high-throughput crystallography of protein-ligand complexes. Acta Crystallogr. D Biol. Crystallogr 2004;60:1355–1363. [PubMed: 15272157]
17. Kleywegt GJ, Jones TA. Detection, delineation, measurement and display of cavities in macromolecular structures. Acta Crystallogr. D Biol. Crystallogr 1994;50:178–185. [PubMed: 15299456]
18. Fraternali F, Cavallo L. Parameter optimized surfaces (POPS): analysis of key interactions and conformational changes in the ribosome. Nucleic Acids Res 2002;30:2950–2960. [PubMed: 12087181]
19. Scott EE, Spatzenegger M, Halpert JR. A truncation of 2B subfamily cytochromes P450 yields increased expression levels, increased solubility, and decreased aggregation while retaining function. Arch. Biochem. Biophys 2001;395:57–68. [PubMed: 11673866]
20. Tsuprun VL, Myasoedova KN, Berndt P, Sograf ON, Orlova EV, Chernyak V, Archakov AI, Skulachev VP. Quaternary structure of the liver microsomal cytochrome P-450. FEBS Lett 1986;205:35–40. [PubMed: 3743769]
21. Fang X, Kobayashi Y, Halpert JR. Stoichiometry of 7-ethoxycoumarin metabolism by cytochrome P450 2B1 wild-type and five active-site mutants. FEBS Lett 1997;416:77–80. [PubMed: 9369237]
22. Poulos TL, Howard AJ. Crystal structures of metyrapone- and phenylimidazole-inhibited complexes of cytochrome P-450cam. Biochemistry 1987;26:8165–8174. [PubMed: 3442650]
23. Hernandez CE, Kumar S, Liu H, Halpert JR. Investigation of the role of cytochrome P450 2B4 active site residues in substrate metabolism based on crystal structures of the ligand-bound enzyme. Arch. Biochem. Biophys 2006;455:61–67. [PubMed: 17027909]

NIH-PA Author Manuscript

NIH-PA Author Manuscript

NIH-PA Author Manuscript

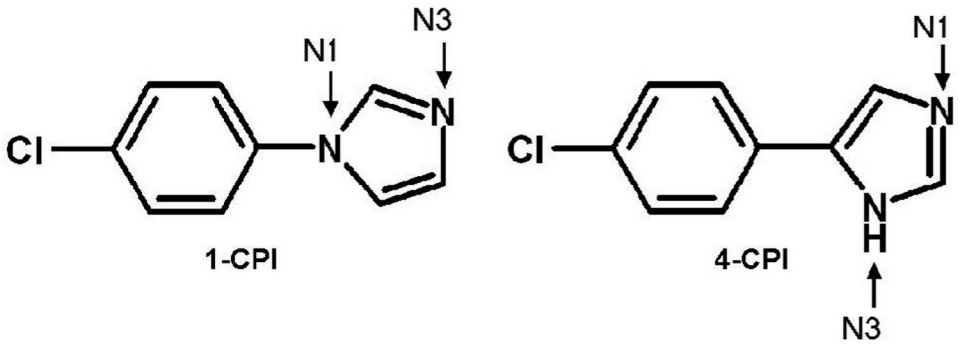

Figure 1.
The chemical structures of 1-CPI and 4-CPI. The numbering of nitrogen atoms is indicated.

NIH-PA Author Manuscript

NIH-PA Author Manuscript

NIH-PA Author Manuscript

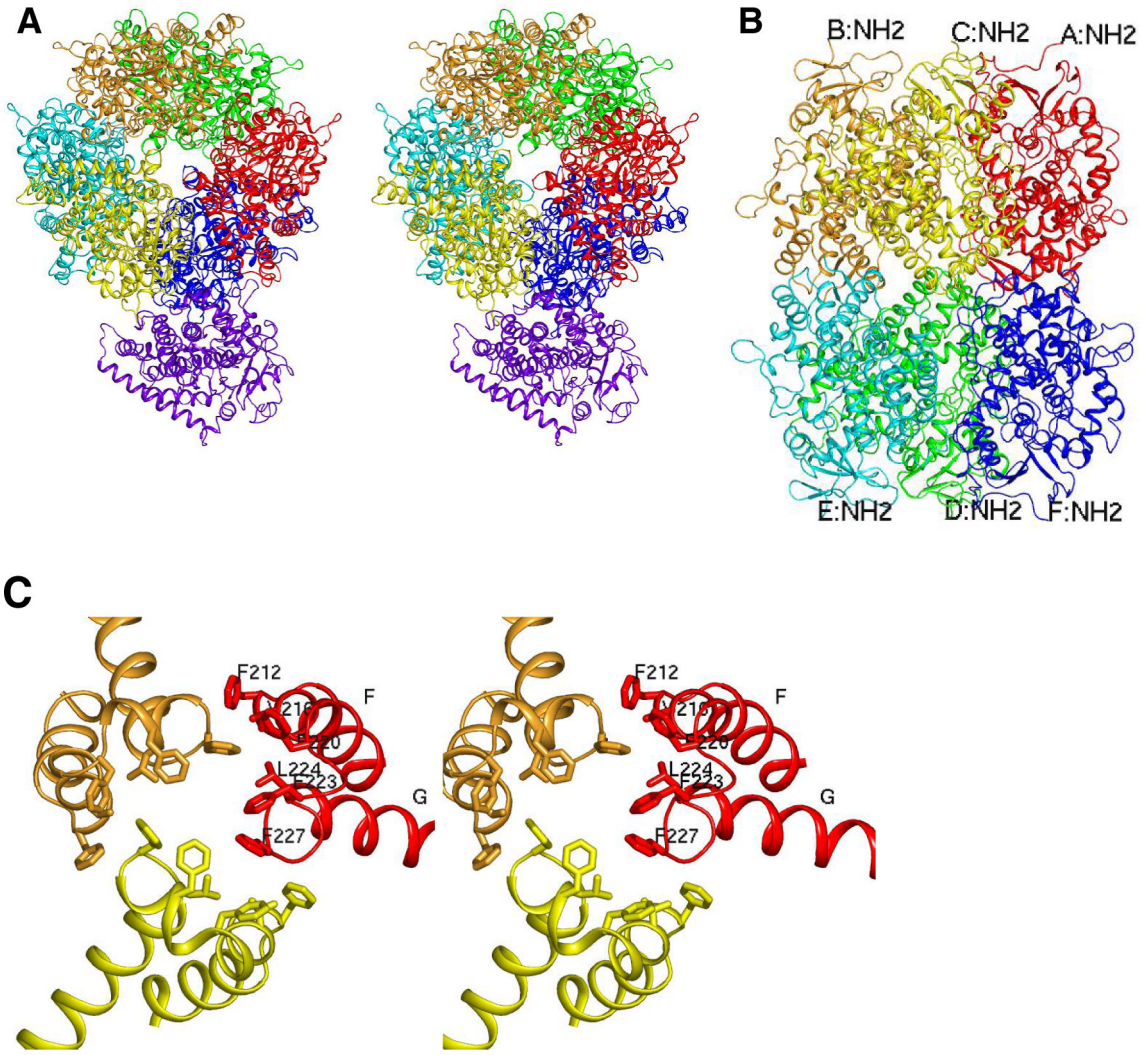

Figure 2.

(A) Divergent stereo view of the seven copies of 2B4/1-CPI in the asymmetric unit. The seven molecules are shown as ribbon diagrams and colored *red* (molecule A), *orange* (B), *yellow* (C), *green* (D), *cyan* (E), *blue* (F), and *purple* (G), respectively. The view is along the 3-fold axis of the hexamer. (B) Side view of the hexamer. The color scheme is the same as in (A), and N-termini are indicated. (C) Divergent stereo view of hydrophobic interactions around the 3-fold axis of trimer ABC. Molecules A, B, and C are colored *red*, *orange*, *yellow*, respectively. The side chains of F212, V216, F220, F223, L224, and F227 are shown as *sticks*. These residues and helices F and G are labeled in molecule A.

NIH-PA Author Manuscript

NIH-PA Author Manuscript

NIH-PA Author Manuscript

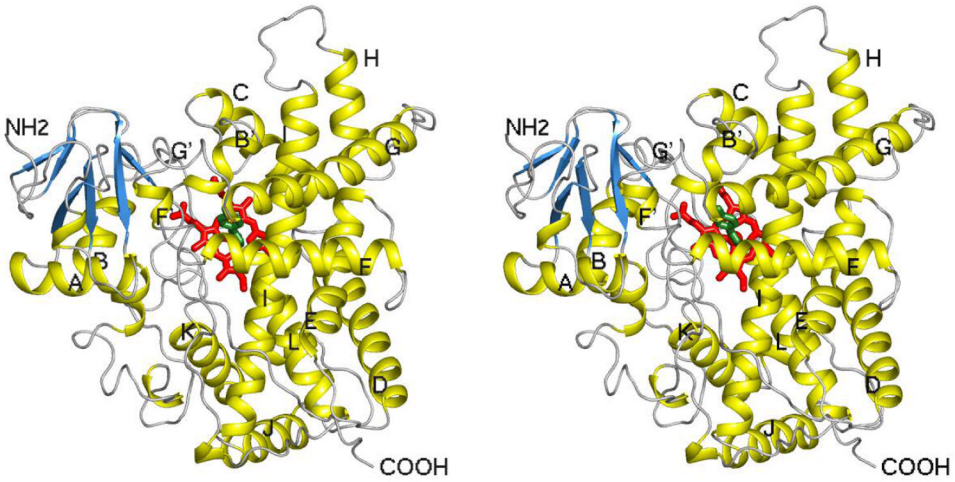

Figure 3.

Divergent stereo view of the 2B4/1-CPI complex (molecule A). Helices and strands are colored *yellow* and *blue*, respectively. The termini and major helices are labeled. Heme and 1-CPI are shown as *red* and *forest sticks*, respectively.

NIH-PA Author Manuscript

NIH-PA Author Manuscript

NIH-PA Author Manuscript

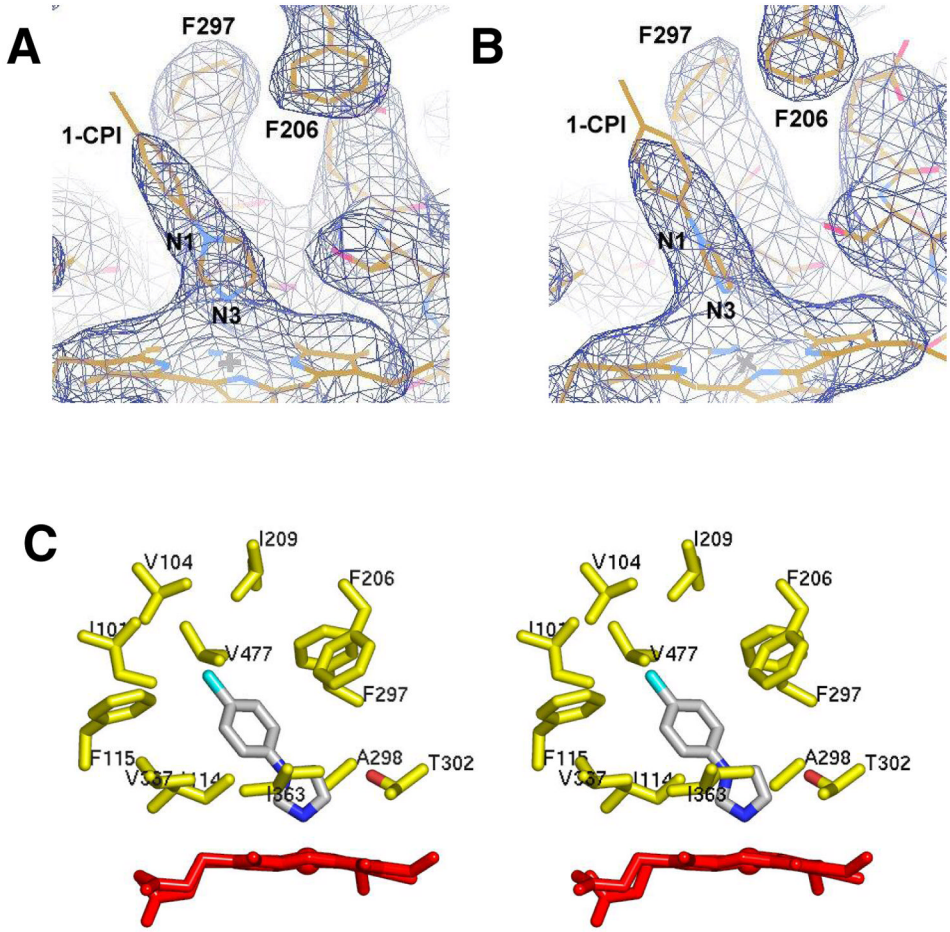

Figure 4.

Electron density map around 1-CPI in the active site of molecule A (A), which has strong density for 1-CPI, and molecule G (B), which has weak density for 1-CPI. The σA-weighted 2|Fo| - |Fc| map is contoured at 1σ and shown as blue mesh around the 1-CPI ligand and adjacent residues, and the heme. F206, F297, and 1CPI are labeled. The nitrogen atoms (N1 and N3) of the imidazole are indicated. (C) Divergent stereo view of 1-CPI in the active site of molecule A. Side chains of residues within a generous 5 Å contact distance from 1-CPI are shown as sticks and colored by elements (*yellow* carbon, *red* oxygen, and *blue* nitrogen). The carbon atoms of 1-CPI are colored *gray*, and the chlorine is colored *cyan*. The heme is shown as *red sticks*.

NIH-PA Author Manuscript

NIH-PA Author Manuscript

NIH-PA Author Manuscript

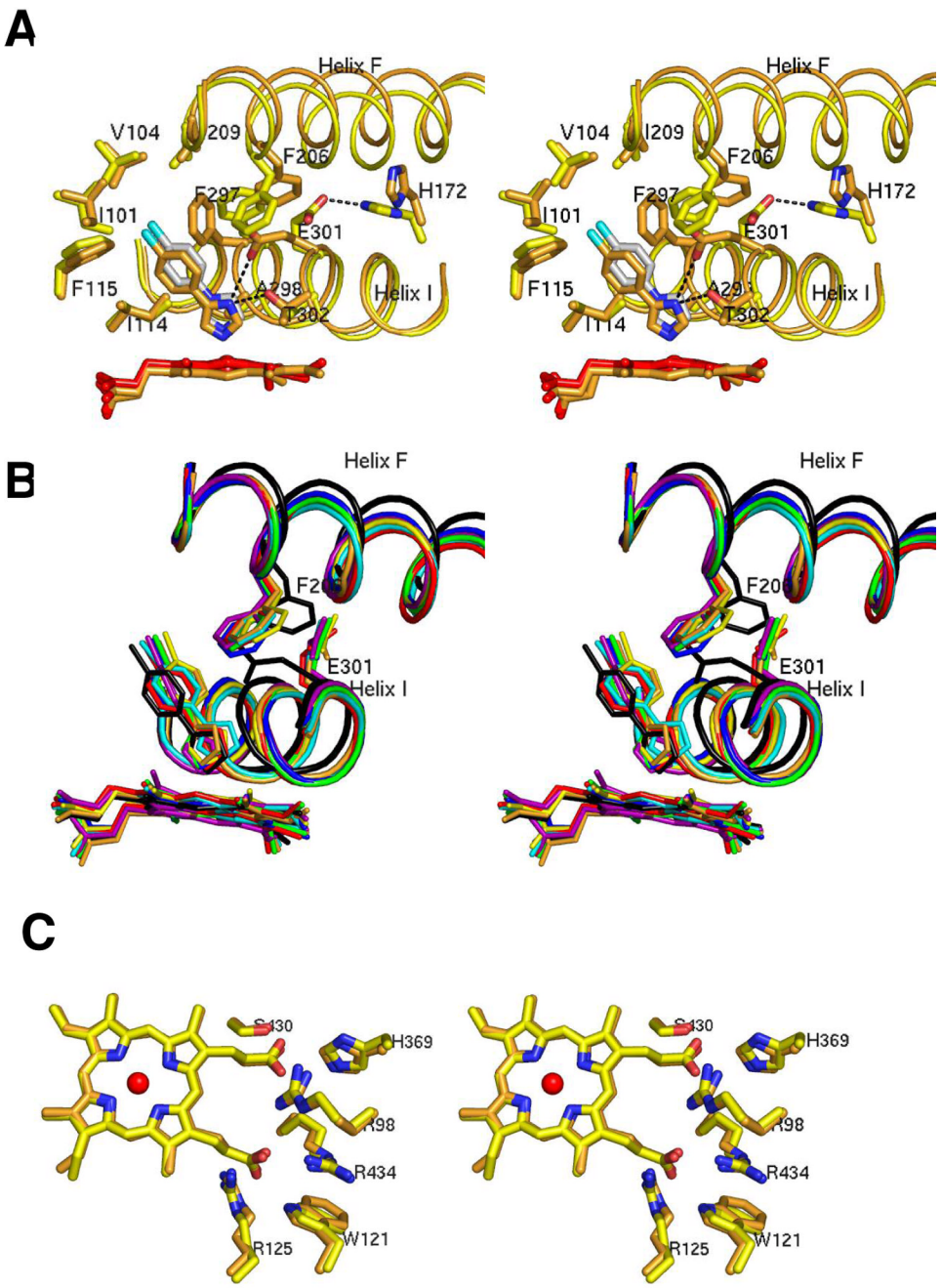

Figure 5.

Divergent stereo views for superposition of the 2B4/1-CPI and 2B4/4-CPI structures. (A) The 2B4/4-CPI structure superposed onto the 2B4/1-CPI (molecule A). Side chains of residues within a generous 5 Å contact distance from the ligands are shown as *sticks* and colored by elements (*orange/yellow* carbon in 2B4/4-CPI or 2B4/1-CPI, *red* oxygen, *blue* nitrogen, and *cyan* chlorine). The carbon atoms of 1-CPI are colored *gray*. Heme is shown as *red* (2B4/1-CPI) or *orange* (2B4/4-CPI) *sticks*. Helices F and I are labeled. (B) Overlay of 2B4/4-CPI and 7 molecules of 2B4/1-CPI in the asymmetric unit. The 2B4/4-CPI structure is colored *black*. The seven molecules of 2B4/1-CPI are colored *red, orange, yellow, green, cyan, blue*, and *purple*, respectively. (C) Heme coordination in 2B4/1-CPI (molecule A) and 2B4/4-CPI. Heme

NIH-PA Author Manuscript

NIH-PA Author Manuscript

NIH-PA Author Manuscript

and side chains of residues involved in coordination of heme propionates are shown as *sticks* and colored by elements (*yellow* carbon, *red* oxygen, and *blue* nitrogen) in 2B4/1-CPI. These residues in the 2B4/4-CPI structure are also shown, and their carbon atoms are colored *orange*. The iron is displayed as a *red sphere*.

NIH-PA Author Manuscript

NIH-PA Author Manuscript

NIH-PA Author Manuscript

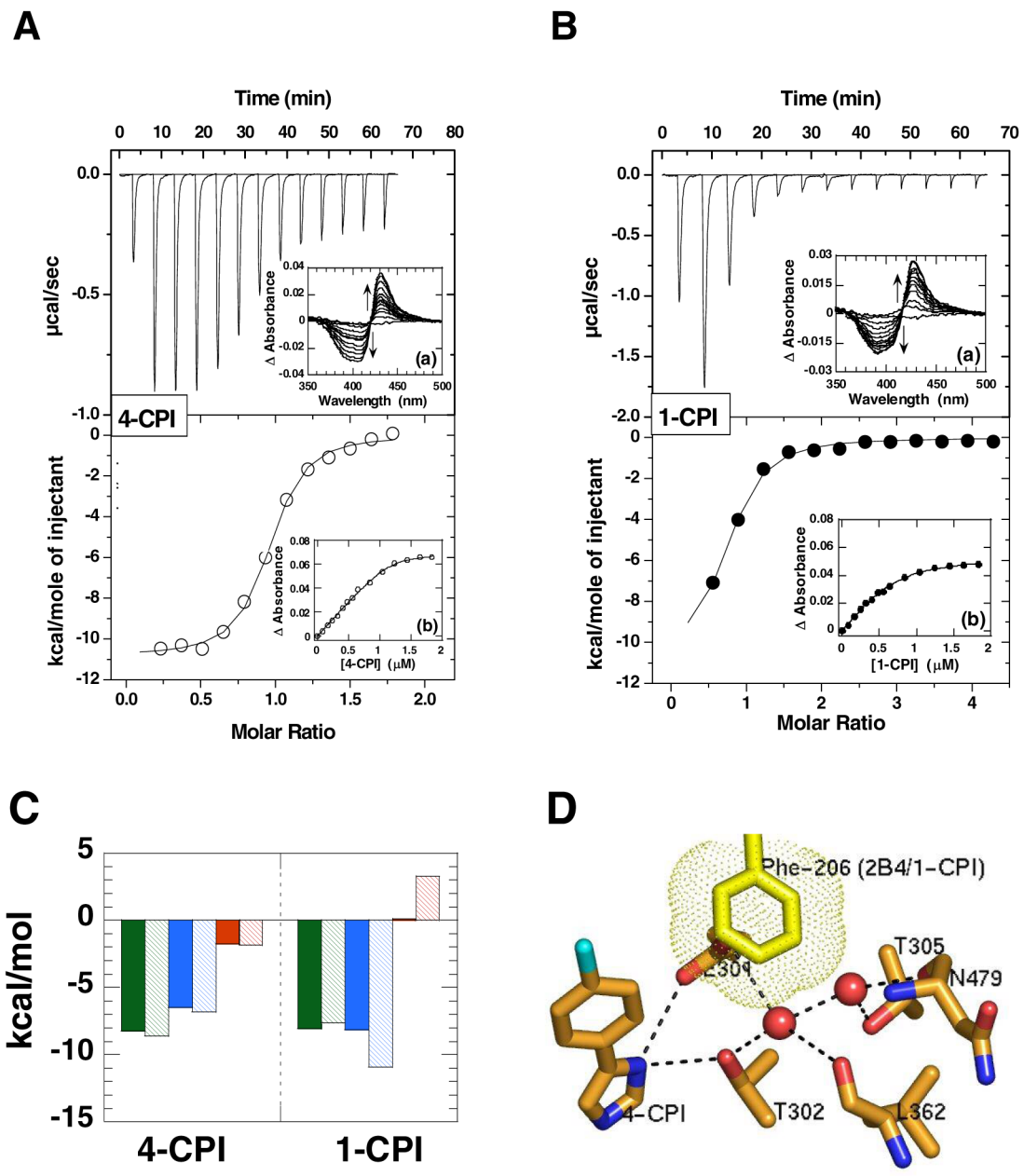

Figure 6.

ITC and spectral studies of 4-CPI (A) and 1-CPI (B) binding to the F206A mutant. The upper panels show the enthalpy changes, and the lower panels are the resulting integrated enthalpy data fit to a single binding site model. The equilibrium difference spectra data are shown in the upper panels (*Inset-a*). The spectral data were fit to the "tight binding" equation, yielding the binding curve shown in the lower panels (*Inset-b*). (C) Thermodynamic signatures of 4-CPI and 1-CPI binding to 2B4dH(H226Y) (10) (solid bars) and F206A (hatched bars) are compared. Binding free energy (ΔG), *green*; change in enthalpy (ΔH), *blue*; change in entropy ($-T\Delta S$), *red*. (D) The network of 8 hydrogen bonds in the 2B4/4-CPI structure. 4-CPI, Leu-362, Asn-479, and the side chains of Glu-301, Thr-302, and Thr-305 are shown as sticks and colored by elements (*orange* carbon, *red* oxygen, *blue* nitrogen, and *cyan* chlorine). Two waters are shown as *red* spheres. Hydrogen bonds are indicated by dashed lines. This network of hydrogen

NIH-PA Author Manuscript

NIH-PA Author Manuscript

NIH-PA Author Manuscript

bonds must be diminished in the 2B4/1-CPI complex, because the new position of the Phe-206 side chain, which is shown as *yellow* sticks, requires the displacement of two water molecules. The van der Waals radius of the Phe-206 side chain is indicated by small dots.

NIH-PA Author Manuscript

NIH-PA Author Manuscript

NIH-PA Author Manuscript

Table 1

Data collection and refinement statistics

Crystals	1[c]	2
Construct	2B4dH(H226Y)	2B4dH(H226Y)
Complex	1-CPI	1-CPI
Space group	$P2_12_12_1$	$P2_12_12_1$
Unit cell (Å) a, b, c	140.0, 147.3, 238.5	137.9, 145.9, 237.0
Data collection		
SSRL beamline	11-1	11-1
Wavelength (Å)	0.98	0.98
Resolution range[a] (Å)	50 - 3.2 (3.28 - 3.2)	50 - 3.2 (3.28 - 3.2)
Total observations[a]	322,694 (24,448)	277,382 (16,387)
Unique reflections[a]	81,299 (5,996)	77,001 (5,216)
Completeness[a]	99.4 (100)	97.1 (90.3)
Redundancy[a]	4.0 (4.1)	3.6 (3.1)
Mean ((I)/sd(I))	9.7 (1.1)	11.7 (1.2)
R_{sym}[a,b]	0.11 (0.831)	0.093 (0.939)
Refinement		
Resolution range (Å)	30.0-3.2	30.0-3.2
R factor (%)	23.3	24.0
R_{free} (%)	31.1	30.9
Average B value (Å^2) A, B, C, D, E, F, G chain	90, 107, 116, 104, 117, 123, 124	89, 98, 104, 97, 115, 119, 114
rms deviations	0.005	0.005
Bond lengths (Å)	0.005	0.005
Bond angles (°)	1.14	1.18

[a] Values for the outer resolution shell of data are given in parentheses.

[b] $R_{sym} = \Sigma \mid I_i - I_m \mid / \Sigma I_i$, where I_i is the intensity of the measured reflection and I_m is the mean intensity of all symmetrically related reflections.

[c] Atomic coordinates refined with this dataset were deposited in the Protein Data Bank and used for presenting the structure.

NIH-PA Author Manuscript

NIH-PA Author Manuscript

NIH-PA Author Manuscript

Table 2

Affinity of 4-CPI and 1-CPI binding to P450 2B4dH

	2B4dH(H226Y) (10)		F206A	
	K_D (μM)	K_S (μM)	K_D (μM)	K_S (μM)
4-CPI	0.89	0.04	0.47	0.04
1-CPI	1.25	0.13	2.56	0.16

Note: the dissociation constants K_D and K_S were obtained from ITC and spectral titration experiments, respectively.